Tunable single-photon diode by chiral quantum physics

Wei-Bin Yan,[1,2] Wei-Yuan Ni,[3] Jing Zhang,[2] Feng-Yang Zhang,[2,*] and Heng Fan[4,†]
[1]*College of Physics and Engineering, Qufu Normal University, Qufu 273165, China*
[2]*School of Physics and Materials Engineering, Dalian Nationalities University, Dalian 116600, China*
[3]*School of Science, Changchun University of Science and Technology, Changchun 130022, China*
[4]*Beijing National Laboratory for Condensed Matter Physics, Institute of Physics, Chinese Academy of Sciences, Beijing 100190, China*

(Received 14 March 2018; revised manuscript received 5 June 2018; published 30 October 2018)

We investigate a single-photon diode realized by a one-dimensional waveguide chirally coupled to N spatially separated Λ-type three-level emitters. An external laser is introduced to drive the emitters. The single photons moving in opposite directions show different transmission probabilities, which underpins the diode behavior. In the case of a single emitter, the single-photon diode works well at specific frequency points, which are tunable by the external laser. In the case of multiple emitters, the optimal-working-frequency point of the diode can be turned to a broad band.

DOI: 10.1103/PhysRevA.98.043852

I. INTRODUCTION

Optical diodes, which allow unidirectional propagation of light, require the ability to break Lorentz reciprocity [1]. Nonreciprocity in light propagation has been extensively studied by various physical mechanisms [2–39]. Single photons are considered as the ideal carriers for quantum information. The single-photon optical diode [15,28–32], with low loss, is an indispensable element for future quantum networks [40], which is prerequisite for optical quantum information and quantum computation.

Recently, the nonreciprocity in single-photon propagation has been well studied by chiral quantum optics, such as the single-photon diode [31,39], single-photon circulator [37,38], and single-photon routing [24,36,39]. In chiral quantum optics, the emitter is driven by the photons propagating in opposite directions with different strengths [20,31,34,35,38,41–57]. This could be underpinned by the spin-momentum locking of the transversely confined light and the polarization-dependent dipole transitions of the emitter. The single-photon diodes realized work well at given frequency points. If the input frequency point is greatly altered, the devices should be actively reconfigured. The investigation of the largely tunable single-photon diode, in which the working frequency point can be adjusted, should be interesting. In addition, it is an open problem to realize a single-photon diode with optimal working frequency in broad bands.

In this paper, we propose a scheme to realize a largely tunable single-photon diode that works well over broad frequency bands. In our scheme, the photon is largely confined in a one-dimensional (1D) waveguide, which is chirally coupled to spatially separated three-level emitters. The system composed by a one-dimensional (1D) waveguide chirally coupled to spatially separated emitters has been extensively studied [45–53,55]. In particular, the Bragg reflection [46,55], entanglement generation [45,48,49], and self-organization [50] have been investigated by a 1D waveguide chirally coupled to spatially separated two-level emitters. By chirally coupling a 1D waveguide to a nonlinear cavity and a two-level atom, the single-photon dark state has been achieved [51]. Here we focus on the asymmetrical single-photon transmission, which is underpinned by both the chiral coupling and the emitter's decay to the environment. We first study in detail the case of a single emitter and show that the optimal working frequency of the diode is at specific points. These points are tunable by programming and actively adjusting the parameters of the external laser. Note that the tunable single-photon circulator composed by two waveguides chirally coupled to a single emitter has been realized in Ref. [37]. The authors in Refs. [30,38,39] have showed that the emitter chirally coupled to two waveguides shows the diode behavior. Our tunable diode containing one waveguide displays more convenience in practice. Besides, in our scheme, the emitter's final state is the same as its initial state, which provides convenience to the recycling. We then show that by chirally coupling a 1D waveguide to multiple spatially separated emitters, the optimal working frequency of the tunable single-photon diode is in broad bands.

II. MODEL AND HAMILTONIAN

We consider N identical Λ-type three-level emitters chirally coupled to a 1D waveguide, as shown in Fig. 1. We use x_i to label the coordinate of the ith emitter. The states of the ith emitter are denoted by $|j\rangle_i$ $(j = a, b, c)$, with the corresponding level frequency ω_j. We take $\omega_b = 0$ for reference. The right- and left-moving guided photons are coupled to the transition $|b\rangle_i \leftrightarrow |a\rangle_i$ with strengths g_R and g_L, respectively. The coupling strengths are assumed to be independent of photon wave number, which is equivalent to the Weisskopf–Wigner approximation. For simplicity and without generality, we assume $g_R \geqslant g_L$. In the ideal chiral

*zhangfy@dlnu.edu.cn
†hfan@iphy.ac.cn

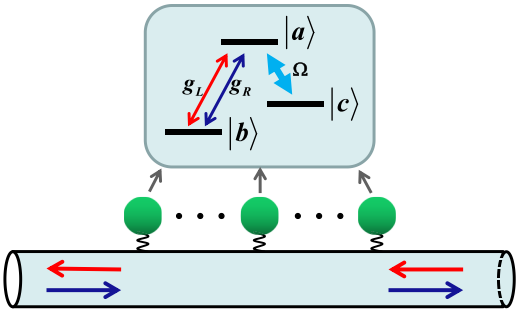

FIG. 1. Schematic configuration of the single-photon diode. A 1D waveguide is chirally coupled to N spatially separated Λ-type three-level emitters. The emitters are driven by the external laser.

coupling case, the photon is perfectly circularly polarized at the positions of the emitters and the polarization is orthogonal for the opposite propagation. Consequently, the level transition $|b\rangle_i \leftrightarrow |a\rangle_i$ can be solely coupled to the photon moving in one direction. To measure the chiral coupling character, we bring in the parameter $C = |\frac{\Gamma_R-\Gamma_L}{\Gamma_R+\Gamma_L}|$. The parameters $\Gamma_R = \frac{g_R^2}{v_g}$ and $\Gamma_L = \frac{g_L^2}{v_g}$ account for the spontaneous emissions from the emitter's excitation into the waveguide's right- and left-moving channels, respectively. The sign v_g denotes the group velocity of the guided photon. Obviously, $C = 0$ when $\Gamma_R = \Gamma_L$, $0 < C < 1$ when $\Gamma_R \neq \Gamma_L$, and $C = 1$ in the ideal-chiral-coupling case. We employ an external laser beam with frequency ω_L and Rabi frequency Ω to drive the level transition $|c\rangle_i \leftrightarrow |a\rangle_i$ by frequency selection. We assume that the transition frequency between the levels $|a\rangle_i$ and $|c\rangle_i$ is below the cutoff frequency of the waveguide and hence the guided photon is decoupled to the transition $|a\rangle_i \leftrightarrow |c\rangle_i$. When $\Omega \neq 0$, the system can be considered as a 1D waveguide chirally coupled to dressed three-level emitters. Within the rotating-wave approximation, the time-independent Hamiltonian governing the system is [58,59]

$$\begin{aligned} H = &-i\int dx[a_R^\dagger(x)\partial_x a_R(x) - a_L^\dagger(x)\partial_x a_L(x)] \\ &+ \sum_{i=1,\ldots,N}\left[\left(\omega_a - i\frac{\gamma_a}{2}\right)\sigma_i^{aa} + (\omega_c+\omega_L)\sigma_i^{cc}\right] \\ &+ \sum_{\substack{m=R,L\\ i=1,\ldots,N}}\left[g_m\int dx\delta(x-x_i)a_m^\dagger(x_i)\sigma_i^{ba}\right. \\ &\left. + \Omega\sigma_i^{ca} + \text{H.c.}\right], \end{aligned} \tag{1}$$

where $\sigma_i^{kl} = |k\rangle_i\langle l|$ $(k,l = a,\ b,\ c)$ are the raising, lowering, and energy-level population operators of the ith emitter. The operator $a_R^\dagger(x)$ $[a_L^\dagger(x)]$ creates a right- (left-) moving photon in the waveguide at the site x. The parameter γ_a accounts for the decay from the level $|a\rangle_i$ to the environment, such as the spontaneous emission to the free space. We have taken $\hbar = 1$, and the photonic group velocity $v_g = 1$. The first line of the Hamiltonian (1) denotes the free propagation of the guided photon. The second line is the emitter's energy including the decay to the environment, which is represented by adding the imaginary part $-i\frac{\gamma_a}{2}$ to the corresponding level energy in the quantum jump picture. Here we have assumed that the states $|b\rangle_i$ and $|c\rangle_i$ are long-lived states, and $|a\rangle_i$ is the excited state. The third line represents the coupling of the waveguide photon to the emitters. The first term in the forth line describes the interaction between the external laser and the emitters. "H.c." stands for Hermitian conjugate.

We consider that, initially, a photon with wave number k is injected into the waveguide and all the emitters are in the state $|b\rangle_i$. The frequency of the guided photon is far from the cutoff frequency of the waveguide so that the photonic dispersion relation is approximately linearized. In the single-excitation sector, the system scattering eigenstate has the form of

$$\begin{aligned} |\Psi\rangle = &\left\{\int dx[\alpha_R(x)a_R^\dagger(x) + \alpha_L(x)a_L^\dagger(x)]\right. \\ &\left. + \sum_{i=1,\ldots,N}\beta_i\sigma_i^{ab} + \sum_{i=1,\ldots,N}\zeta_i\sigma_i^{cb}\right\}|\phi\rangle, \end{aligned} \tag{2}$$

where $\alpha_R(x)$, $\alpha_L(x)$, β_i and ζ_i are the probability amplitudes. The state $|\phi\rangle$ means that all the emitters are in the state $|b\rangle_i$ and zero photons are in the 1D waveguide. The first and second terms in Eq. (2) indicate that the 1D waveguide contains one right- and left-moving photons, respectively. The third and forth terms indicate that the ith emitter is in state $|a\rangle_i$ and $|c\rangle_i$, respectively. The probability amplitudes can be obtained from the eigenequation $H|\Psi\rangle = E|\Psi\rangle$, with eigenvalue $E = v_g|k|$ (see Appendix A for details).

III. SINGLE-PHOTON DIODE REALIZED BY SINGLE EMITTER

First, we study single-photon scattering by a single emitter chirally coupled to a 1D waveguide. We assume that the emitter is coupled to the waveguide at the site $x = 0$. When the input photon is injected from the left side of the waveguide, we label the single-photon-transmission and -reflection probability amplitudes with t_R and r_R, respectively. The subscript R denotes that the input photon is right moving. Similarly, if the photon is input from the right side, the corresponding amplitudes are represented by t_L and r_L, respectively. The amplitudes are obtained as (see Appendix B for details)

$$\begin{aligned} t_R &= \frac{\Delta_k\left(\delta_k + i\frac{\Gamma_R-\Gamma_L-\gamma_a}{2}\right)+\Omega^2}{\Delta_k\left(\delta_k - i\frac{\Gamma_R+\Gamma_L+\gamma_a}{2}\right)+\Omega^2}, \\ t_L &= \frac{\Delta_k\left(\delta_k + i\frac{\Gamma_L-\Gamma_R-\gamma_a}{2}\right)+\Omega^2}{\Delta_k\left(\delta_k - i\frac{\Gamma_R+\Gamma_L+\gamma_a}{2}\right)+\Omega^2}, \\ r_L &= r_R = \frac{i\sqrt{\Gamma_R\Gamma_L}\Delta_k}{\Delta_k\left(\delta_k - i\frac{\Gamma_R+\Gamma_L+\gamma_a}{2}\right)+\Omega^2}, \end{aligned} \tag{3}$$

where $\delta_k = \omega_{ab} - v_g|k|$ and $\Delta_k = \Delta - \delta_k$ are detunings, with $\Delta = \omega_{ac} - \omega_L$. When $\Gamma_R = \Gamma_L = \Gamma$, we can easily find

$$t_R = t_L = \frac{\Delta_k\left(\delta_k - i\frac{\gamma_a}{2}\right)+\Omega^2}{\Delta_k\left(\delta_k - i\frac{\gamma_a}{2} - i\Gamma\right)+\Omega^2},$$

agreeing with the outcomes derived in a 1D waveguide symmetrically coupled to a three-level emitter [59]. Here we focus on the case $\Gamma_R \neq \Gamma_L$. The only difference between t_R and t_L is the signs Γ_R and Γ_L in the numerators. This can be understood from the symmetry of the system, which implies that the

expression of t_L (r_L) can be obtained by exchanging the signs Γ_R and Γ_L in t_R (r_R). If the emitter's decay to the environment is neglected, i.e., $\gamma_a = 0$, the single-photon-transmission probabilities $T_R = |t_R|^2$ and $T_L = |t_L|^2$ are equal, although $t_R \neq t_L$. The single-photon diode cannot be achieved. When the decay rate γ_a is not negligible, T_R and T_L differ from each other due to the chiral coupling. However, the reflection probabilities $R_R = |r_R|^2$ and $R_L = |r_L|^2$ are equal in any case. We label $R = R_R = R_L$. This can be understood from the perspective of mode conversion. The photonic right- and left-moving modes, with the same frequency, are considered as two degenerate modes. The input photon moving towards the emitter will be absorbed by the emitter and then be emitted into the waveguide or into the environment. If the propagation direction of the emitted guided photon is opposite to the input photon, the photon in the left-moving (right-moving) mode is converted to the right-moving (left-moving) photon. The conversion efficiencies are essentially the reflection probabilities. Obviously, the conversion efficiency from the left-moving mode to the right-moving mode is equal to the efficiency from the right-moving mode to the left-moving mode. This can also be understood from the outcomes in Ref. [60], in which the single-photon mode conversion by an emitter coupled to two continuum modes and the environment is well investigated. If the photon is emitted into the environment after scattering, we consider that the input photon mode is converted to environmental mode. The transmission implies that the input photon is not converted to other modes. Therefore, the transmission probability is essentially $T_m = 1 - C_{m\to\text{envi}} - C_{R\leftrightarrow L}$ ($m = R, L$), where $C_{m\to\text{envi}}$ is the conversion efficiency from mode m to the environmental mode and $C_{R\leftrightarrow L}$ is the conversion efficiency between the left- and right-moving modes. The conversion efficiency $C_{m\to\text{envi}}$ relates to the parameters γ_a and g_m. The efficiency $C_{R\to\text{envi}}$ is not equal to $C_{L\to\text{envi}}$ in the chiral coupling case, which results in $T_R \neq T_L$. Therefore, both the chiral coupling and the emitter's decay to the environment are necessary to realize the single-photon diode.

If the external laser is shut off, our scheme is a 1D waveguide coupled to a two-level emitter. It is known that a single-photon diode can be realized by a chirally coupled two-level emitter [39]. Here we give a detailed investigation on the single-photon transport property. In the symmetrical coupling case, i.e., $\Gamma_R = \Gamma_L$, the single-photon scattering by a two-level emitter has been extensively studied. It is known that when the emitter's decay to the environment is neglected, the single photon moving towards the emitter will be fully reflected by interference in the resonance case [61]. In the chiral-coupling case, the input single photon cannot be fully reflected. This has been predicted in Ref. [39] by qualitative analysis and observed in experiment [55]. For completeness, here we give a detailed analysis of this case. The maximum value of R is obtained as $1 - C^2$ in the resonance case. In Fig. 2(a), we plot the single-photon reflection probabilities scattered by a two-level emitter. The spectra are shaped like the Lorentzian line. As the difference between Γ_R and Γ_L increases, the maximum value of $R = C_{R\leftrightarrow L}$ decreases. The conversion efficiency $C_{R\leftrightarrow L}$ reaches unity only when $\Gamma_R = \Gamma_L$. The quantum critical coupling condition [62] cannot be satisfied for any nonzero value of γ_a in the symmetrical-coupling case. In the chiral-coupling case, when

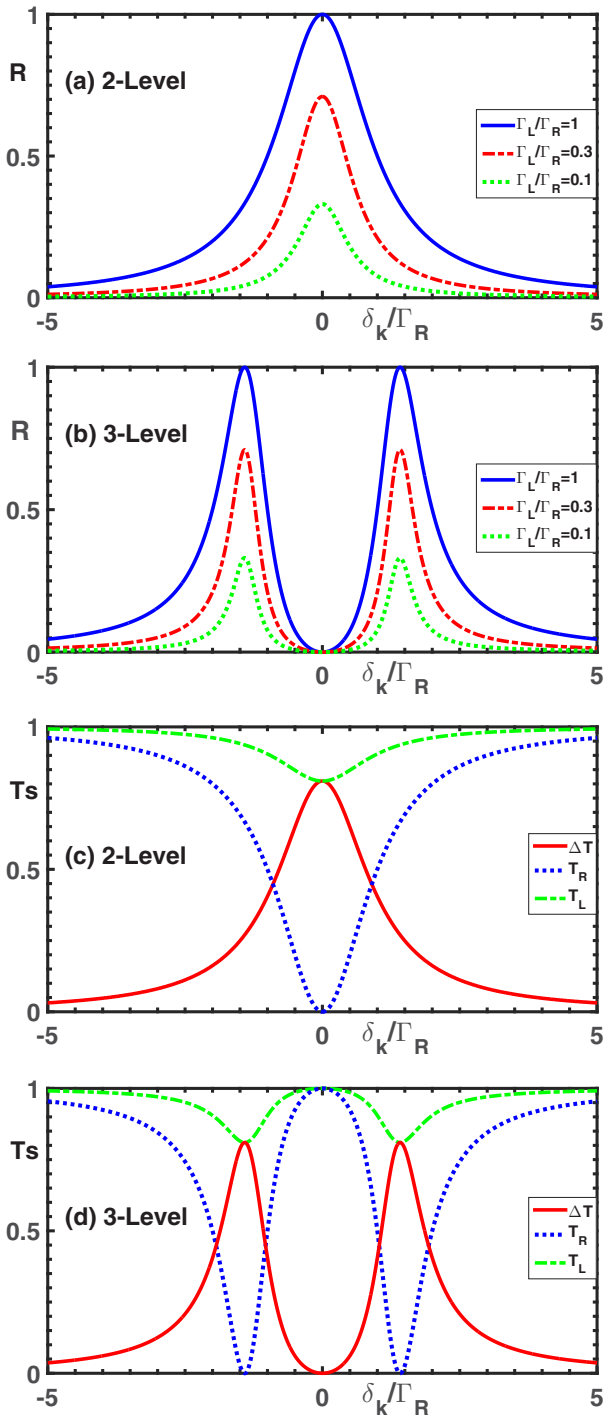

FIG. 2. Single-photon transport properties against the detuning δ_k. Panels (a) and (b) show the reflection probability R when $\gamma_a = 0$. Panels (c) and (d) show the transmission probabilities T_R, T_L, and ΔT when $\gamma_a = \Gamma_R - \Gamma_L$. Panels (a) and (c) represent the case of a single two-level emitter, panels (b) and (d) denote the case of a single Λ-type three-level emitter. The green dotted, red dashed dotted, and blue solid lines in panels (a) and (b) denote the situations $\Gamma_L/\Gamma_R = 0.1$, $\Gamma_L/\Gamma_R = 0.3$, and $\Gamma_L/\Gamma_R = 1$, respectively. The red solid, blue dotted, and green dashed dotted lines in panels (c) and (d) denote the probabilities ΔT, T_R, and T_L when $\Gamma_L/\Gamma_R = 0.1$, respectively. The other parameters in panels (b) and (d) are $\Omega^2/\Gamma_R = 2$ and $\Delta = 0$. The axis label Ts in panels (c) and (d) denotes the transmission probabilities.

$\delta_k = 0$ and $\gamma_a = \Gamma_R - \Gamma_L$, we obtain $T_R = 0$, $T_L = (\frac{\Gamma_R - \Gamma_L}{\Gamma_R})^2$, and $R = \frac{\Gamma_L}{\Gamma_R}$. The resonant single photon injected into the left port of the waveguide cannot be received from the right port due to the quantum critical coupling. However, the single photon injected into the right port will be received from the left port with a near unity probability when $C \to 1$. In the ideal chiral coupling case, the photon injected from the left side will be completely decayed into the environment. The photon injected from the right hand will be completely transmitted because it is decoupled to the emitter. The difference between the transmission probabilities corresponding to the opposite transport directions is

$$\Delta T = |T_R - T_L| = \frac{4\gamma_a(\Gamma_R - \Gamma_L)}{4\delta_k^2 + (\gamma_a + \Gamma_R + \Gamma_L)^2}.$$

We can see that ΔT reaches its maximum value only when $\delta_k = 0$ and $\gamma_a = \Gamma_R - \Gamma_L$. Figure 2(c) shows the transmission probabilities T_R, T_L, and ΔT against δ_k when $\Omega = 0$, $\Gamma_L/\Gamma_R = 0.1$, and $\gamma_a = \Gamma_R - \Gamma_L$.

When the external laser is turned on, our scheme is a 1D waveguide chirally coupled to a Λ-type three-level emitter. In this case, the single-photon-transmission and -reflection probabilities have been obtained in Eqs. (3). When $\Delta_k = 0$, the single photon will be fully transmitted in any case due to the interference, which corresponds to electromagnetically induced transparency (EIT). This is similar to the symmetrical-coupling case [59]. We plot the single-photon reflection probabilities against the detuning δ_k when $\gamma_a = 0$ in Fig. 2(b). The spectra split due to the interaction between the emitter and the laser. Similar to the two-level emitter, the chiral coupling reduces the maximum value of R. When $\gamma_a = \Gamma_R - \Gamma_L$ and $\delta_k = [\Delta \pm (\Delta^2 + 4\Omega^2)^{1/2}]/2$, we obtain $T_R = 0$ and $T_L = (\frac{\Gamma_R - \Gamma_L}{\Gamma_R})^2$. In this case,

$$\Delta T = \frac{4\gamma_a(\Gamma_R - \Gamma_L)\Delta_k^2}{4(\Delta_k\delta_k + \Omega^2)^2 + \Delta_k^2(\gamma_a + \Gamma_R + \Gamma_L)^2}$$

reaches its maximum value. In Fig. 2(d) we plot the single-photon transmission probabilities in the case of a single Λ-type three-level emitter. The maximum values of ΔT and T_L are equal to the corresponding values compared with the case of a single two-level emitter. However, the Λ-type three-level emitter underpins the tunable single-photon diode.

To ensure the diode works well, the frequency point of the single photon cannot be arbitrary. For a two-level emitter, the single photon should be nearly resonant to the emitter, i.e., $\delta_k \simeq 0$. For a Λ-type three-level emitter, the single-photon frequency point should satisfy the relation $\delta_k \simeq [\Delta \pm (\Delta^2 + 4\Omega^2)^{1/2}]/2$. The latter shows the advantage that it is largely tunable. For various values of the input frequency points, we can adjust the frequency and Rabi frequency of the laser to satisfy this relation. Although this cannot be satisfied for any arbitrary value of the input frequency, it can be satisfied in a large range of values. This feasible range is enough to obtain a largely tunable single-photon diode. We plot the probabilities T_R and ΔT against the laser parameters in Fig. 3. It shows that, for a given input frequency point, the single-photon diode works well at various values of the laser frequencies and Rabi frequencies. This provides the convenience to the selection of laser parameters.

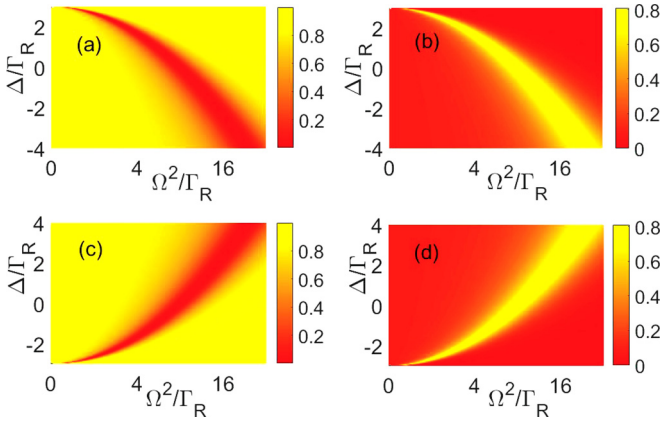

FIG. 3. Single-photon-transmission probabilities against the frequency and Rabi frequency of the external laser. Panels (a) and (c) show the probability T_R. Panels (b) and (d) show ΔT. We take $\delta_k/\Gamma_R = 3$ in panels (a) and (b), $\delta_k/\Gamma_R = -3$ in panels (c) and (d). The other parameters are $\Gamma_L/\Gamma_R = 0.1$ and $\gamma_a/\Gamma_R = 0.9$.

The tunable single-photon diode can be understood in the dressed-state representation. Our scheme can be considered as a 1D waveguide chirally coupled to a three-level V-type emitter [30,59] with states $|b\rangle$, $|+\rangle$, and $|-\rangle$. The dressed states $|\pm\rangle$ are the eigenstates of the Hamiltonian

$$H_{AL} = \omega_a\sigma^{aa} + (\omega_c + \omega_L)\sigma^{cc} + \Omega(\sigma^{ac} + \sigma^{ca}),$$

with corresponding eigenenergies

$$E_{AL}^{\pm} = \omega_a - \frac{\Delta \pm \sqrt{\Delta^2 + 4\Omega^2}}{2}.$$

The condition $\delta_k = [\Delta \pm (\Delta^2 + 4\Omega^2)^{1/2}]/2$ implies that the single photon resonantly drives the transition $|b\rangle \leftrightarrow |\pm\rangle$.

The decay-matching condition $\gamma_a = |\Gamma_R - \Gamma_L|$ plays an important role. The rate γ_a mainly relates to the environment surrounding the emitter. The decay rates Γ_R and Γ_L relate to the position of the emitter relative to the waveguide. For the diode composed by an emitter coupled to two waveguides [30,39], one of the waveguide channels plays the role of the environment.

Our scheme also shows certain advantages of the single-photon switch. The control of the single-photon transport in 1D waveguide has been extensively studied, such as the investigations in Refs. [58,59,61,63–65]. It is known that when the emitter's decay to the environment is neglected, the single-photon-transmission probability can be zero or unity by controlling the emitter. However, when the emitter's decay is considered, this perfect outcome cannot be realized. In our scheme, we can ensure the single photon is fully transmitted by EIT with the correct choice of the laser frequency. Similarly, by adjusting the parameters of the laser, we can ensure the single photon cannot be transmitted by quantum critical coupling. It is interesting that the emitter's decay to the environment has been considered for these operations.

IV. SINGLE-PHOTON DIODE REALIZED BY MULTIPLE EMITTERS

We proceed to study the case of multiple emitters to realize the tunable single-photon diode working well in broad frequency bands. We assume that the emitters are equally

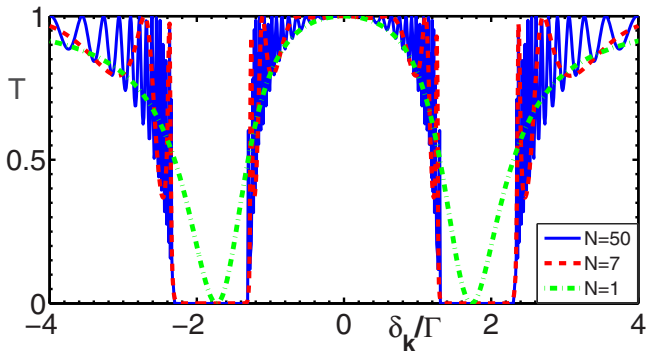

FIG. 4. Single-photon-transmission probability against the detuning δ_k. The green dashed dotted, red dashed, and blue solid lines denote the situations $N = 1$, $N = 7$, and $N = 50$, respectively. The parameters are $\Delta = 0$, $\Omega^2/\Gamma = 3$, and $kL = 2m\pi + \pi/2$ with m integer.

separated and take $x_i = iL$. To investigate the single-photon transport property in detail, we first study the case where the emitters are symmetrically coupled to the 1D waveguide, i.e., $g_R = g_L = g$. It is known that the photon transport property scattered by spatially separated emitters [66–73] shows essential difference compared with one emitter. The nonreciprocal transmission of the single photon cannot be realized in the symmetrical coupling case. Therefore, we label $t = t_R = t_L$ and $r = r_R = r_L$. The expressions of the single-photon transmission and reflection probability amplitudes are (see Appendix C 1 for details)

$$r = \frac{iAe^{ikL}}{(1 - iA)e^{-ikL} - \sin[(N-1)\beta]\csc(N\beta)},$$
$$t = \frac{\sin\beta\csc(N\beta)e^{-ikNL}}{(1 - iA)e^{-ikL} - \sin[(N-1)\beta]\csc(N\beta)}, \tag{4}$$

with

$$A = \frac{\Gamma\Delta_k}{\Delta_k\delta_k + \Omega^2},$$
$$\cos\beta = \cos kL - A\sin kL.$$

The parameter $\Gamma = \frac{g^2}{v_g}$. Here we have not considered the emitters' decay to the environment. It is easy to verify $|r|^2 + |t|^2 = 1$. The single-photon transport property can be studied by inserting

$$\sin(N\beta) = \sum_{n=0}^{(N-1)/2} C_N^{2n+1}(-1)^n \times \cos^{N-1-2n}\beta\sin^{2n+1}\beta$$

into the amplitudes (4). The expressions (4) can be simplified by Markovian approximation, in which the value of kL is assumed constant.

To see the details of the single-photon-scattering property, we plot single-photon-transmission probability $T = |t|^2$ against the detuning δ_k in Fig. 4. The zero value of transmission probability represents that the single photon is completely reflected. The single photon is scattered by the emitters and the interference among the wave functions of the scattered photon arises. The two dips of the spectra become flat and show box-like shape when N is large. For a small value

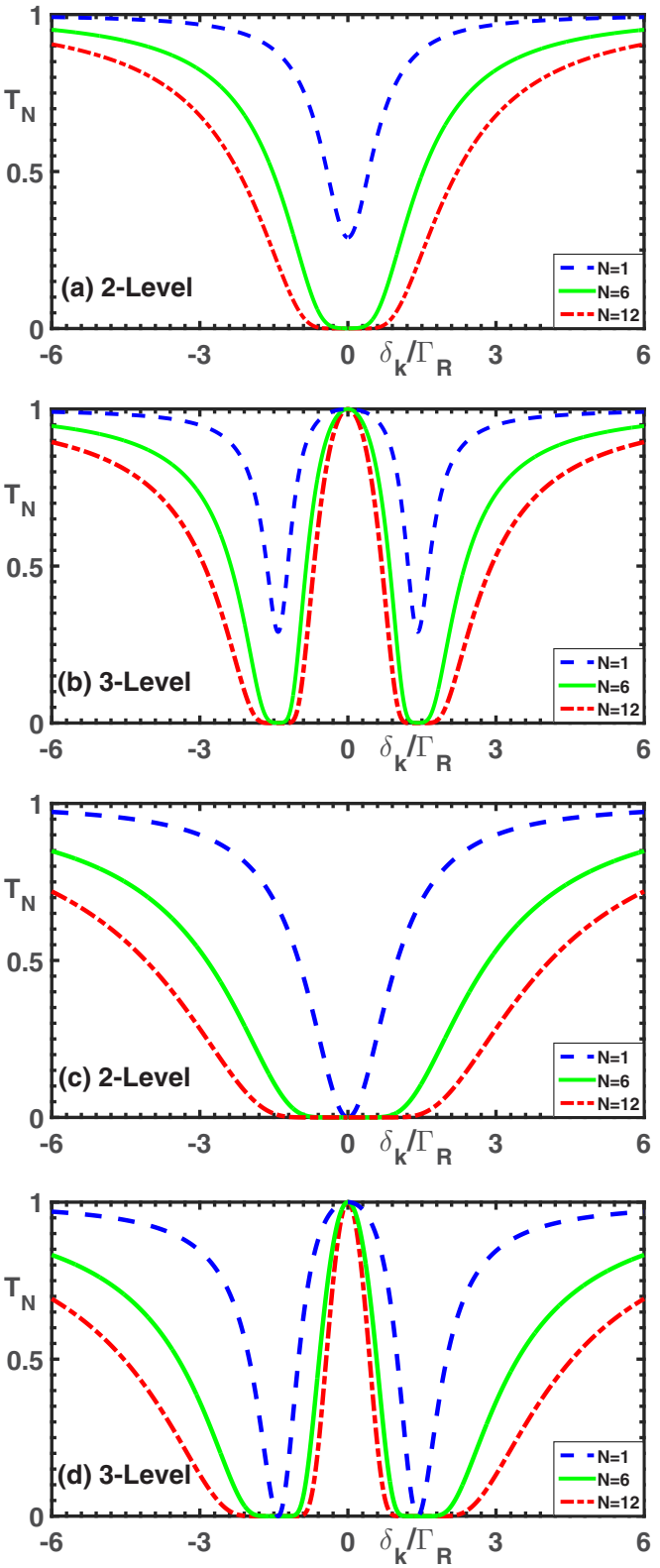

FIG. 5. Transmission probability of the right-moving single photon against the detuning δ_k. The blue dashed, green solid, and red dashed dotted lines denote the situations $N = 1$, $N = 6$, and $N = 12$, respectively. We take $\Omega = 0$ in panels (a) and (c), and take $\Omega^2/\Gamma_R = 2$ and $\Delta = 0$ in panels (b) and (d). In panels (a) and (b), the decay rate $\gamma_a/\Gamma_R = 0.3$. In panels (c) and (d), we take $\gamma_a/\Gamma_R = 1$.

of N, our lines show similar behavior as in Ref. [66]. The box-like dips show almost no change with the increasing value of N. When N is large enough, the lineshapes show high-frequency oscillation. This is similar to the single-photon transport property in 1D coupled cavity array doped by two-level emitters [71], in which the spectra have one dip.

We proceed to study the nonreciprocal transmission of the single photon when the spatially separated emitters are chirally coupled to the waveguide. We consider the ideal chiral coupling case as done in Refs. [24,30,36,39]. In this case, the dipole polarizations corresponding to the transition $|b\rangle_i \leftrightarrow |a\rangle_i$ are orthogonal to the polarization of the left-propagate guided photon, i.e., $g_L = 0$. The photon injected from the right side of the waveguide will be fully transmitted because it is decoupled to the waveguide. The transmission probability amplitude of the right-moving photon is obtained as (see Appendix C 2 for details)

$$t_N = \left[\frac{\Delta_k\left(\delta_k + i\frac{\Gamma_R-\gamma_a}{2}\right)+\Omega^2}{\Delta_k\left(\delta_k - i\frac{\Gamma_R+\gamma_a}{2}\right)+\Omega^2}\right]^N. \tag{5}$$

The phase shift, which can be adjusted by the parameters of the laser, is imprinted on the transmitted single photon. When the condition of EIT is satisfied, the phase shift is canceled. Because the right-moving photon cannot be converted into left-moving photon, the interference among the photonic wave functions is absent, which is different from the symmetrical-coupling case. The single photon is sequentially scattered by the spatially separated emitters. Therefore, the amplitude (5) does not relate to the emitters' positions. However, the locations of the emitters cannot be arbitrary because they are strictly limited by the polarization of the guided photons.

We plot the transmission probability of the right-moving photon, $T_N = |t_N|^2$, in Fig. 5. The lines in Figs. 5(a) and 5(c) represent the case of multiple two-level emitters. Figures 5(b) and 5(d) denote the case of multiple Λ-type three-level emitters. In Figs. 5(a) and 5(b), the values of γ_a and Γ_R differ greatly. The leakage probability of the single photon to the environment increases rapidly with increasing N. The diode composed by one emitter cannot work well although the single photon is resonant to the single emitter. However, when N is large, the diode works well for both resonant and nonresonant cases, as shown in Figs. 5(a) and 5(b). Therefore, in the multiple-emitter case, it is not necessary to ensure the parameters γ_a and Γ_R are equal. This would be much more easily achieved in practice. For all the cases in Fig. 5, the single-photon diode that works well in broad frequency band can be achieved by a 1D waveguide chirally coupled to spatially separated emitters. Similar to the single-emitter case, the positions of the band relate to the laser parameters. The width of the band increases as N increases. By the correct choice of system parameters, the value of N up to the order of ten is enough to realize the broad bands for preventing the right-moving single photon.

We have assumed that the state $|c\rangle_i$ is long lived. If $|c\rangle_i$ is an excited state, the decay from state $|c\rangle_i$ to the environment can be incorporated by introducing an extra non-Hermitian term $-i\frac{\gamma_c}{2}\sigma^{cc}$ into the Hamiltonian (1), with γ_c corresponding decay rate. Consequently, the sign Δ_k in Eqs. (3) and

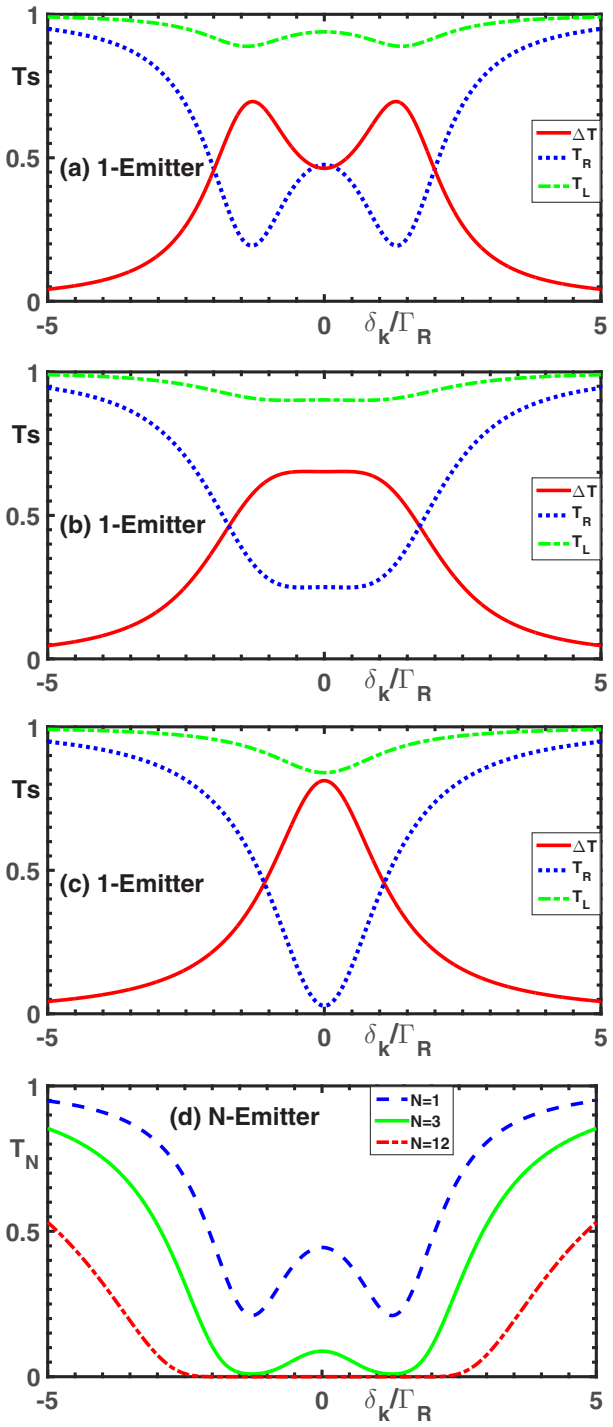

FIG. 6. Single-photon transport properties against the detuning δ_k, in which the decay from the state $|c\rangle_i$ to the environment has been considered. Panels (a)–(c) show the single-emitter case. We take $\gamma_c/\Gamma_R = 0.9$, 2, and 10 in panels (a)–(c), respectively. All the other parameters in panels (a)–(c) are the same as in Fig. 2(d). The same as Fig. 2(d), the red solid, blue dotted, and green dashed dotted denote the probabilities ΔT, T_R, and T_L, respectively. Panel (d) corresponds to the case in Fig. 5(d). Except for $\gamma_c = \Gamma_R$, all the other parameters in panel (d) are the same as in Fig. 5(d). The blue dashed, green solid, and red dashed dotted lines denote the cases of $N = 1$, 3, and 12, respectively. The axis label Ts in panels (a)–(c) denotes the transmission probabilities.

(5) should be replaced with $\Delta_k + i\frac{\gamma_c}{2}$. In this case, the Λ-type emitters can also be replaced by three-level emitters in cascade configuration [65]. Figure 6 plots the single-photon transmission probabilities, in which the decay from level $|c\rangle_i$ to the environment is considered. Figures 6(a)–6(c) denote the case of a single emitter. The only difference between Figs. 6(a)–6(c) and Fig. 2(d) is the consideration of the decay γ_c. We cannot observe EIT at the point $\Delta_k = 0$. The increasing γ_c slowly increases the values of T_R at the points $\delta_k = [\Delta \pm (\Delta^2 + 4\Omega^2)^{1/2}]/2$, and rapidly decreases the values of T_R at the point $\Delta_k = 0$. In the single-emitter case, for certain value of γ_c, the significant asymmetrical single-photon transmission can be realized in a broad frequency band. When γ_c is large enough, the shape of the lines in Fig. 6(c) is similar to that in the case of a single two-level emitter. This can be understood by the fact that the transition between $|c\rangle_i$ and $|a\rangle_i$ is approximatively decoupled to the laser when γ_c is large enough. Figure 6(d) plots T_N in the case where N emitters are ideally chirally coupled to the 1D waveguide, in which we take $\gamma_c = \Gamma_R$. Compared with the situation of $\gamma_c = 0$ in Fig. 5(d), the value of T_R at point $\Delta_k = 0$ decreases rapidly with the increasing N. When N is large enough, the peak of the lines disappears and the dip becomes broader.

V. CONCLUSIONS

We propose a scheme to investigate the tunable single-photon diode working well in broad frequency bands. The diode is composed by spatially separated emitters chirally coupled to a 1D waveguide. The single-photon diode is underpinned by both the chirally coupling and the decay from the emitter to the environment. To make the single-photon diode work well, the frequency of the single photon must satisfy certain conditions. For a single Λ-type three-level emitter, the diode can work well at various frequency points by adjusting the external laser parameters. Different from the few-photon diode in Ref. [12], the single-photon diode property is not affected by the nonlinear effect in the Λ-type three-level emitter. For multiple spatially separated emitters, the diode works well in broad frequency bands. Our scheme can be used to control single photons by integrated optical circuits.

ACKNOWLEDGMENTS

W.B.Y. was supported by the National Science Foundation of China under Grants No. 11505023 and No. 11447134. F.Y.Z. was supported by the National Science Foundation of China under Grants No. 11505024 and No. 11447135, the Natural Science Foundation of Liaoning Province under Grant No. 20180550944, and the Fundamental Research Funds for the Central Universities Grant No. wd01151. H.F. was supported by National Key R & D Program of China (Grants No. 2016YFA0302104 and No. 2016YFA0300600), NSFC (Grants No. 91536108 and No. 11774406), Strategic Priority Research Program of Chinese Academy of Sciences (Grant No. XDB28000000).

APPENDIX A: EIGENEQUATIONS

In the appendix, we obtain the amplitudes in Eqs. (3)–(5) by using the technique in Refs. [58,59,69]. The system Hamiltonian can be easily diagonalized in the single-excitation sector. From eigenequation, we find a set of equations

$$\begin{aligned}
(-i\partial_x - k)\alpha_R(x) + \sum_{i=1,\ldots,N} g_R\delta(x - x_i)\beta_i &= 0,\\
(i\partial_x - k)\alpha_L(x) + \sum_{i=1,\ldots,N} g_L\delta(x - x_i)\beta_i &= 0,\\
\delta_k\beta_i + g_R\alpha_R(x_i) + g_L\alpha_L(x_i) + \Omega\zeta_i &= 0,\\
-\Delta_k\zeta_i + \Omega\beta_i &= 0.
\end{aligned} \tag{A1}$$

Here we neglected the emitter's decay to the environment. We make an ansatz that the spatial dependent probability amplitudes of the right- and left-moving photons have the forms of $\alpha_R(x) = \sum_{i=0,\ldots,N} t_i e^{ikx}\theta(x_{i+1} - x)\theta(x - x_i)$ and $\alpha_L(x) = \sum_{i=0,\ldots,N} r_i e^{-ikx}\theta(x_{i+1} - x)\theta(x - x_i)$, respectively. The function $\theta(x)$ is the Heaviside step function, and t_i (r_i) denotes the probability amplitude of the right-moving (left-moving) photon at the immediate right of the ith emitter. Hence, we obtain

$$\begin{aligned}
-i(t_i' - t_{i-1}' e^{ikL}) + g_R\beta_i &= 0,\\
i(r_i' - r_{i-1}' e^{-ikL}) + g_L\beta_i &= 0,\\
\delta_k\beta_i + \frac{g_R}{2}(t_i' + t_{i-1}' e^{ikL}) + \frac{g_L}{2}(r_i' + r_{i-1}' e^{-ikL}) + \Omega\zeta_i &= 0,\\
-\Delta_k\zeta_i + \Omega\beta_i &= 0.
\end{aligned} \tag{A2}$$

Here we have taken $t_i' = t_i e^{ikx_i}$ and $r_i' = r_i e^{-ikx_i}$ for the sake of simplicity. By eliminating β_i and ζ_i in Eqs. (A2), we find

$$\begin{pmatrix} t_N' \\ r_N' \end{pmatrix} = M^N \begin{pmatrix} t_0' \\ r_0' \end{pmatrix}, \tag{A3}$$

with the following elements of matrix M:

$$\begin{aligned}
M_{11} &= \frac{\Delta_k\left(\delta_k + i\frac{\Gamma_L}{2} + i\frac{\Gamma_R}{2}\right) + \Omega^2}{\Delta_k\left(\delta_k + i\frac{\Gamma_L}{2} - i\frac{\Gamma_R}{2}\right) + \Omega^2} e^{ikL},\\
M_{12} &= \frac{i\Delta_k\sqrt{\Gamma_L\Gamma_R}}{\Delta_k\left(\delta_k + i\frac{\Gamma_L}{2} - i\frac{\Gamma_R}{2}\right) + \Omega^2} e^{-ikL},\\
M_{21} &= \frac{-i\Delta_k\sqrt{\Gamma_L\Gamma_R}}{\Delta_k\left(\delta_k + i\frac{\Gamma_L}{2} - i\frac{\Gamma_R}{2}\right) + \Omega^2} e^{ikL},\\
M_{22} &= \frac{\Delta_k\left(\delta_k - i\frac{\Gamma_L}{2} - i\frac{\Gamma_R}{2}\right) + \Omega^2}{\Delta_k\left(\delta_k + i\frac{\Gamma_L}{2} - i\frac{\Gamma_R}{2}\right) + \Omega^2} e^{-ikL}.
\end{aligned}$$

Here we have used the condition that the emitters are equally separated and $x_i - x_{i-1} = L$. When the single photon is injected from the left side, $t_0 = 1$ and $r_N = 0$. The single-photon-transmission and -reflection probability amplitudes are represented by $t_R = t_N$ and $r_R = r_0$, respectively. When the photon is injected from the right side, $r_N = 1$ and $t_0 = 0$. The transmission and reflection probability amplitudes are $t_L = r_0$ and $r_L = t_N$, respectively. Under given initial condition, the single-photon-transmission and -reflection probabilities can be found by solving Eq. (A3).

APPENDIX B: SINGLE-EMITTER CASE

In the case of a single emitter, the distance L is meaningless and hence the terms $e^{\pm ikL}$ in the elements of matrix M should be discarded. We assume that the coordinate of the single emitter is $x = 0$. If the photon is injected from the left side, we obtain

$$\begin{pmatrix} t_R \\ 0 \end{pmatrix} = M \begin{pmatrix} 1 \\ r_R \end{pmatrix}, \tag{B1}$$

Therefore, the amplitudes T_R and r_R are

$$\begin{aligned} t_R &= \frac{\Delta_k\left(\delta_k - i\frac{\Gamma_L}{2} + i\frac{\Gamma_R}{2}\right) + \Omega^2}{\Delta_k\left(\delta_k - i\frac{\Gamma_L}{2} - i\frac{\Gamma_R}{2}\right) + \Omega^2}, \\ r_R &= \frac{i\Delta_k\sqrt{\Gamma_L\Gamma_R}}{\Delta_k\left(\delta_k - i\frac{\Gamma_L}{2} - i\frac{\Gamma_R}{2}\right) + \Omega^2}. \end{aligned} \tag{B2}$$

Similarly, if the photon is injected from the right side, we obtain

$$\begin{pmatrix} r_L \\ 1 \end{pmatrix} = M \begin{pmatrix} 0 \\ t_L \end{pmatrix}, \tag{B3}$$

and hence

$$\begin{aligned} t_L &= \frac{\Delta_k\left(\delta_k + i\frac{\Gamma_L}{2} - i\frac{\Gamma_R}{2}\right) + \Omega^2}{\Delta_k\left(\delta_k - i\frac{\Gamma_L}{2} - i\frac{\Gamma_R}{2}\right) + \Omega^2}, \\ r_R &= r_L. \end{aligned} \tag{B4}$$

The decay from the emitter's level $|a\rangle_i$ into the environment is incorporated by replacing δ_k with $\delta_k - i\frac{\gamma_a}{2}$. Having considered the decay, the amplitudes (3) are obtained.

APPENDIX C: MULTIPLE-EMITTER CASE

1. Symmetrical-Coupling Case

When the 1D waveguide is symmetrically coupled by N emitters, the elements of matrix M become

$$\begin{aligned} M_{11} &= (1 + iA)e^{ikL}, \\ M_{12} &= iAe^{-ikL}, \\ M_{21} &= -iAe^{ikL}, \\ M_{22} &= (1 - iA)e^{-ikL}. \end{aligned}$$

The analytical expression of M^N can be found by using the method in Ref. [74]. The eigenvalues u_1 and u_2 of the matrix M satisfy the equation $u_1^2 - 2\cos\beta u_1 + 1 = 0$ and $u_2^2 - 2\cos\beta u_2 + 1 = 0$, and M^N is found as a function of β:

$$M^N = \frac{\sin N\beta}{\sin\beta}M - \frac{\sin(N-1)\beta}{\sin\beta}I. \tag{C1}$$

The relation (C1) can be verified by the mathematical induction. The transmission and reflection probability amplitudes in Eqs. (4) are obtained by solving

$$\begin{pmatrix} te^{ikNL} \\ 0 \end{pmatrix} = \left[\frac{\sin N\beta}{\sin\beta}M - \frac{\sin(N-1)\beta}{\sin\beta}I\right]\begin{pmatrix} 1 \\ r \end{pmatrix}. \tag{C2}$$

2. Ideal Chiral-Coupling Case

When $g_L = 0$, the elements of matrix M become

$$\begin{aligned} M_{11} &= \frac{\Delta_k\left(\delta_k + i\frac{\Gamma_R}{2}\right) + \Omega^2}{\Delta_k\left(\delta_k - i\frac{\Gamma_R}{2}\right) + \Omega^2}e^{ikL}, \\ M_{22} &= e^{-ikL}, \\ M_{12} &= M_{21} = 0, \end{aligned}$$

The fact that the nondiagonal elements are zero implies that the right-moving (left-moving) photon cannot be converted into the left-moving (right-moving) photon by scattering. The phases of $e^{\pm ikL}$ in M_{11} and M_{22} arises from the forms of t' and r'. The element M_{11} implies that the phase shift of

$$\frac{\Delta_k\left(\delta_k + i\frac{\Gamma_R}{2}\right) + \Omega^2}{\Delta_k\left(\delta_k - i\frac{\Gamma_R}{2}\right) + \Omega^2}$$

is imprinted on the right-moving photon after the photon is scattered by any one of the emitters. The element M_{22} agree with the fact that the left-moving photon is decoupled to the emitters. When the photon is injected from the left side, the Eq. (A3) becomes

$$\begin{pmatrix} t_R e^{ikNL} \\ 0 \end{pmatrix} = P\begin{pmatrix} 1 \\ 0 \end{pmatrix}, \tag{C3}$$

with

$$P = \begin{pmatrix} \left[\frac{\Delta_k\left(\delta_k + i\frac{\Gamma_R}{2}\right) + \Omega^2}{\Delta_k\left(\delta_k - i\frac{\Gamma_R}{2}\right) + \Omega^2}e^{ikL}\right]^N & 0 \\ 0 & e^{-ikNL} \end{pmatrix}.$$

Therefore, the transmission probability amplitude t_R is obtained as

$$t_R = \left[\frac{\Delta_k\left(\delta_k + i\frac{\Gamma_R}{2}\right) + \Omega^2}{\Delta_k\left(\delta_k - i\frac{\Gamma_R}{2}\right) + \Omega^2}\right]^N. \tag{C4}$$

In Eq. (C4) we have not considered the emitters' decay to the environment and hence the right-moving photon is completely transmitted. However, when the decay is considered, the photon can be fully converted into the environment under certain conditions. By replacing δ_k in Eq. (C4) with $\delta_k - i\gamma_a$ the amplitude (5) is obtained. To avoid confusion, we use the sign t_N to label the transmission probability amplitude in Eq. (5).

[1] D. Jalas, A. Petrov, M. Eich, W. Freude, S. Fan, Z. Yu, R. Baets, M Popović, A. Melloni, J. D. Joannopoulos, M. Vanwolleghem, C. R. Doerr, and H. Renner, Nat. Photon. **7**, 579 (2013).

[2] K. Gallo, G. Assanto, K. R. Parameswaran, and M. M. Fejer, Appl. Phys. Lett. **79**, 314 (2001).

[3] H. Lira, Z. Yu, S. Fan, and M. Lipson, Phys. Rev. Lett. **109**, 033901 (2012).

[4] T. R. Zaman, X. Guo, and R. J. Ram, J. Lightwave Technol. **26**, 291 (2008).
[5] L. Bi, J. Hu, P. Jiang, D. H. Kim, G. F. Dionne, L. C. Kimerling, and C. Ross, Nat. Photon. **5**, 758 (2011).
[6] Z. Yu and S. Fan, Nat. Photon. **3**, 91 (2009).
[7] J. Kim, S. Kim, and G. Bahl, Sci. Rep. **7**, 1647 (2017).
[8] J. Kim, M. C. Kuzyk, K. Han, H. Wang, and G. Bahl, Nat. Phys. **11**, 275 (2015).
[9] A. Kamal, J. Clarke, and M. H. Devoret, Nat. Phys. **7**, 311 (2011).
[10] D. L. Sounas, C. Caloz, and A. Alu, Nat. Commun. **4**, 2407 (2013).
[11] D. Roy, Phys. Rev. B **81**, 155117 (2010).
[12] D. Roy, Phys. Rev. A **96**, 033838 (2017).
[13] N. A. Estep, D. L. Sounas, J. Soric, and A. Alu, Nat. Phys. **10**, 923 (2014).
[14] F. Fratini, E. Mascarenhas, L. Safari, J.-P. Poizat, D. Valente, A. Auffèves, D. Gerace, and M. F. Santos, Phys. Rev. Lett. **113**, 243601 (2014).
[15] H. Z. Shen, Y. H. Zhou, and X. X. Yi, Phys. Rev. A **90**, 023849 (2014).
[16] F. Fratini and R. Ghobadi, Phys. Rev. A **93**, 023818 (2016).
[17] Y. Yu, Y. Chen, H. Hu, W. Xue, K. Yvind, and J. Mork, Laser Photon. Rev. **9**, 241 (2015).
[18] X. Gu, A. F. Kockum, A. Miranowicz, Y. X. Liu, and F. Nori, Phys. Rep. **718-719**, 1 (2017).
[19] Y. Shi, Z. Yu, and S. Fan, Nat. Photon. **9**, 388 (2015).
[20] P.-O. Guimond, H. Pichler, A. Rauschenbeutel, and P. Zoller, Phys. Rev. A **94**, 033829 (2016).
[21] A. E. Miroshnichenko, E. Brasselet, and Y. S. Kivshar, Appl. Phys. Lett. **96**, 063302 (2010).
[22] L. Fan, J. Wang, L. T. Varghese, H. Shen, B. Niu, Y. Xuan, A. M. Weiner, and M. Qi, Science **335**, 447 (2012).
[23] N. Bender, S. Factor, J. D. Bodyfelt, H. Ramezani, D. N. Christodoulides, F. M. Ellis, and T. Kottos, Phys. Rev. Lett. **110**, 234101 (2013).
[24] M.-T. Cheng, X.-S. Ma, J.-Y. Zhang, and B. Wang, Opt. Express **24**, 19988 (2016).
[25] F. J. Rodríguez-Fortuño, G. Marino, P. Ginzburg, D. O'Connor, A. Martínez, G. A. Wurtz, and A. V. Zayats, Science **340**, 328 (2013).
[26] B. Peng, S. K. Özdemir, F. Lei, F. Monifi, M. Gianfreda, G. L. Long, S. Fan, F. Nori, C. M. Bender, and L. Yang, Nat. Phys. **10**, 394 (2014).
[27] L. Chang, X. Jiang, S. Hua, C. Yang, J. Wen, L. Jiang, G. Li, G. Wang, and M. Xiao, Nat. Photon. **8**, 524 (2014).
[28] Y. Shen, M. Bradford, and J.-T. Shen, Phys. Rev. Lett. **107**, 173902 (2011).
[29] E. J. Lenferink, G. Wei, and N. P. Stern, Opt. Express **22**, 16099 (2014).
[30] K. Xia, G. Lu, G. Lin, Y. Cheng, Y. Niu, S. Gong, and J. Twamley, Phys. Rev. A **90**, 043802 (2014).
[31] C. Sayrin, C. Junge, R. Mitsch, B. Albrecht, D. O'Shea, P. Schneeweiss, J. Volz, and A. Rauschenbeutel, Phys. Rev. X **5**, 041036 (2015).
[32] X.-W. Xu, A.-X. Chen, Y. Li, and Y.-X. Liu, Phys. Rev. A **95**, 063808 (2017).
[33] R. Mitsch, C. Sayrin, B. Albrecht, P. Schneeweiss, and A. Rauschenbeutel, Nat. Commun. **5**, 5713 (2014).
[34] J. Petersen, J. Volz, and A. Rauschenbeutel, Science **346**, 67 (2014).
[35] B. Le Feber, N. Rotenberg, and L. Kuipers, Nat. Commun. **6**, 6695 (2015).
[36] C.-H. Yan, Yong Li, H. Yuan, and L. F. Wei, Phys. Rev. A **97**, 023821 (2018).
[37] M.-T. Cheng, X. Ma, J.-W. Fan, J. Xu, and C. Zhu, Opt. Lett. **42**, 2914 (2017).
[38] M. Scheucher, A. Hilico, E. Will, J. Volz, and A. Rauschenbeutel, Science **354**, 1577 (2016).
[39] C. Gonzalez-Ballestero, E. Moreno, F. J. Garcia-Vidal, and A. Gonzalez-Tudela, Phys. Rev. A **94**, 063817 (2016).
[40] H. J. Kimble, Nature (London) **453**, 1023 (2008).
[41] P. Lodahl, S. Mahmoodian, S. Stobbe, A. Rauschenbeutel, P. Schneeweiss, J. Volz, H. Pichler, and P. Zoller, Nature (London) **541**, 473 (2017).
[42] T. V. Mechelen and Z. Jacob, Optica **3**, 118 (2016).
[43] F. LeKien and A. Rauschenbeutel, Phys. Rev. A **90**, 023805 (2014).
[44] T. V. Mechelen, T. Thundat, and Z. Jacob, Appl. Phys. Lett. **108**, 061102 (2016).
[45] C. Gonzalez-Ballestero, A. Gonzalez-Tudela, F. J. Garcia-Vidal, and E. Moreno, Phys. Rev. B **92**, 155304 (2015).
[46] F. LeKien and A. Rauschenbeutel, Phys. Rev. A **90**, 063816 (2014).
[47] B. Vermersch, T. Ramos, P. Hauke, and P. Zoller, Phys. Rev. A **93**, 063830 (2016).
[48] I. M. Mirza and J. C. Schotland, Phys. Rev. A **94**, 012302 (2016).
[49] I. M. Mirza and J. C. Schotland, Phys. Rev. A **94**, 012309 (2016).
[50] Z. Eldredge, P. Solano, D. Chang, and A. V. Gorshkov, Phys. Rev. A **94**, 053855 (2016).
[51] F. Zhu, T. Zhao, H. Zhang, G.-X. Li, and Z. Ficek, Phys. Rev. A **95**, 023817 (2017).
[52] F. LeKien and A. Rauschenbeutel, Phys. Rev. A **95**, 023838 (2017).
[53] D. F. Kornovan, M. I. Petrov, and I. V. Iorsh, Phys. Rev. B **96**, 115162 (2017).
[54] T. Li, A. Miranowicz, X. Hu, K. Xia, and F. Nori, Phys. Rev. A **97**, 062318 (2018).
[55] N. V. Corzo, B. Gouraud, A. Chandra, A. Goban, A. S. Sheremet, D. V. Kupriyanov, and J. Laurat, Phys. Rev. Lett. **117**, 133603 (2016).
[56] F. LeKien, T. Ray, T. Nieddu, T. Busch, and S. Nic Chormaic, Phys. Rev. A **97**, 013821 (2018).
[57] F. LeKien, S. S. Hejazi, T. Busch, V. G. Truong, and S. Nic Chormaic, Phys. Rev. A **96**, 043859 (2017).
[58] J.-T. Shen and S. Fan, Phys. Rev. A **79**, 023837 (2009).
[59] D. Witthaut and A. S. Sørensen, New J. Phys. **12**, 043052 (2010).
[60] M. Bradford, K. C. Obi, and J.-T. Shen, Phys. Rev. Lett. **108**, 103902 (2012).
[61] J. T. Shen and S. Fan, Opt. Lett. **30**, 2001 (2005).
[62] J.-T. Shen and S. Fan, Phys. Rev. A **82**, 021802(R) (2010).
[63] L. Zhou, Z. R. Gong, Y. X. Liu, C. P. Sun, and F. Nori, Phys. Rev. Lett. **101**, 100501 (2008).
[64] C.-H. Yan, W.-Z. Jia, and L.-F. Wei, Phys. Rev. A **89**, 033819 (2014).
[65] W.-B. Yan and H. Fan, Phys. Rev. A **90**, 053807 (2014).

[66] G.-Z. Song, E. Munro, W. Nie, F.-G. Deng, G.-J. Yang, and L. C. Kwek, Phys. Rev. A **96**, 043872 (2017).
[67] Z. Liao, H. Nha, and M. S. Zubairy, Phys. Rev. A **94**, 053842 (2016).
[68] Z. Liao, X. Zeng, S. Y. Zhu, and M. S. Zubairy, Phys. Rev. A **92**, 023806 (2015).
[69] T. S. Tsoi and C. K. Law, Phys. Rev. A **80**, 033823 (2009).
[70] Yao-Lung L. Fang and H. U. Baranger, Phys. Rev. A **91**, 053845 (2015).
[71] Y. Chang, Z. R. Gong, and C. P. Sun, Phys. Rev. A **83**, 013825 (2011).
[72] S. Das, V. E. Elfving, F. Reiter, and A. S. Sørensen, Phys. Rev. A **97**, 043837 (2018).
[73] S. Das, V. E. Elfving, F. Reiter, and A. S. Sørensen, Phys. Rev. A **97**, 043838 (2018).
[74] J. M. Bendickson, J. P. Dowling, and M. Scalora, Phys. Rev. E **53**, 4107 (1996).